

pubs.acs.org/JPCB Article

Thermal Transport in Poly(p-phenylene): Anomalous Dimensionality Dependence and Role of π - π Stacking

Cong Yang, Saqlain Raza, Xiaobo Li,* and Jun Liu*



Cite This: J. Phys. Chem. B 2023, 127, 6804-6813

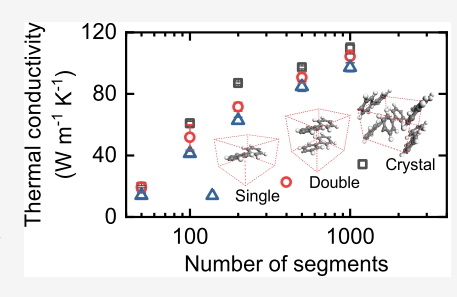


ACCESS |

Metrics & More

Article Recommendations

ABSTRACT: For heat conduction along polymer chains, a decrease in the axial thermal conductivity often occurs when the polymer structure changes from one-dimensional (1D) to three-dimensional (3D). For example, a single extended aliphatic chain (e.g., polyethylene or poly(dimethylsiloxane)) usually has a higher axial thermal conductivity than its double-chain or crystal counterparts because coupling between chains induces strong interchain anharmonic scatterings. Intuitively, for chains with an aromatic backbone, the even stronger π – π stacking, once formed between chains, should enhance thermal transport across chains and suppress the thermal conductivity along the chains. However, we show that this trend is the opposite in poly(p-phenylene) (PPP), a typical chain with an aromatic backbone. Using molecular dynamics



simulations, we found that the axial thermal conductivity of PPP chains shows an anomalous dimensionality dependence where the thermal conductivity of double-chain and 3D crystal structures is higher than that of a 1D single chain. We analyzed the probability distribution of dihedral angles and found that $\pi-\pi$ stacking between phenyl rings restricts the free rotation of phenyl rings and forms a long-range order along the chain, thus enhancing thermal transport along the chain direction. Though possessing a stronger bonding strength and stabilizing the multiple-chain structure, $\pi-\pi$ stacking does not lead to a higher interchain thermal conductance between phenyl rings compared with that between aliphatic chains. Our simulation results on the effects of $\pi-\pi$ stacking provide insights to engineer thermal transport in polymers at the molecular level.

I. INTRODUCTION

Polymers that dissipate heat or tune heat flow on demand¹⁻³ will have significant implications for applications such as flexible electronics, smart textiles, and batteries, thanks to their unparalleled combination of properties. In addition, identifying thermally conductive polymers will substantially improve the thermal performance of polymer composites. To date, advanced engineering of polymers toward high or tunable thermal conductivity remains challenging due to the unsettled relationships among molecular composition/structure, processing conditions, and thermal properties. These relationships are complicated by the highly complex molecular structure and distinct intra- and interchain interactions in polymers. Even with many recent advances in modeling approaches, 8,9 characterization techniques, ^{10–13} and machine learning algorithms, 14-17 significant breakthroughs have yet to be discovered and understanding of thermal transport mechanisms remains elusive. The overarching question now becomes "what molecular features yield high and low thermal conductivity?"

Many molecular features can affect the thermal conductivity in polymers, such as chain orientation, ^{18–20,11} backbone composition, ^{12,21} side chain, ^{22,23} kinks, ²⁴ chain topologies, ^{25–31} and interchain interactions, ^{12,32,33} which have been summarized in a few recent review articles. ^{7,34–38} A large amount of research investigations in this direction in the past two decades were inspired by early theoretical work showing

that a single polyethylene (PE) chain can have a high thermal conductivity comparable to that of metals. ^{39–41} Then, Henry and Chen found that there is a *dimensionality dependence* of the axial thermal conductivity in PE. ⁴² In their simulations, all of the PE chains are well aligned, and when they varied the PE from a single-chain to double-chain and to bulk crystal, the thermal conductivity decreases significantly. They attributed this dependence to interchain coupling. A similar dimensionality dependence was also found in the poly-(dimethysiloxane). ⁴³ This dependence also exists in inorganic materials, ⁴⁴ such as graphene/graphite system, ⁴⁵ but appears controversial in MoS₂ ⁴⁶ and black phosphorus. ⁴⁷ Then, a natural question would be "is this dimensionality dependence universal, at least for polymer chains?"

In this work, we simulated the axial thermal conductivity of conjugated poly(p-phenylene) (PPP) in single-chain, double-chain, and crystal structures to investigate the dimensionality dependence in such molecular systems with aromatic back-

Received: May 4, 2023 Revised: June 27, 2023 Published: July 21, 2023





bone. We selected this system because the π - π stacking between the phenyl rings might provide a different coupling between aromatic chains compared with chains with an aliphatic backbone. In aromatic rings, six p-type orbitals of six carbon atoms split into three bonding molecular orbitals (MOs) and three antibonding MOs that have π -symmetry. Between the aromatic rings, there will also be orbital overlap to form the noncovalent interactions, which assemble the rings into a special stacking structure, called π - π stacking (also called π stacking ^{48,49}). The typical interaction strength of π – π stacking⁵⁰ is in the range of 1–40 kJ mol⁻¹, which is stronger than the strength of van der Waals interactions, 0.4-4 kJ mol⁻¹. Moreover, electrostatic Coulombic interactions play an important role in the π - π stacking. Our results show that PPP molecular systems have an opposite dimensionality dependence compared with that in the aliphatic chains (e.g., PE and poly(dimethysiloxane)). This seemingly counterintuitive result motivates our further investigations into the role of π - π stacking on the structural order along the chain and the interchain thermal conductance. This work proves that dimensionality dependence in polymer chains is not universal and reveals the important role of π - π stacking in the thermal transport of polymers, which provides insights for molecular engineering of thermal conductivity in polymeric materials.

II. SIMULATION METHOD

II.I. Material Models of PPP in Single-Chain, Double-Chain, and Crystal Configurations. We used the all-atom model to describe polymer chains in this work; each atom is treated as a single site and assigned a corresponding mass. Figure 1a depicts the atomic model of a single extended PPP

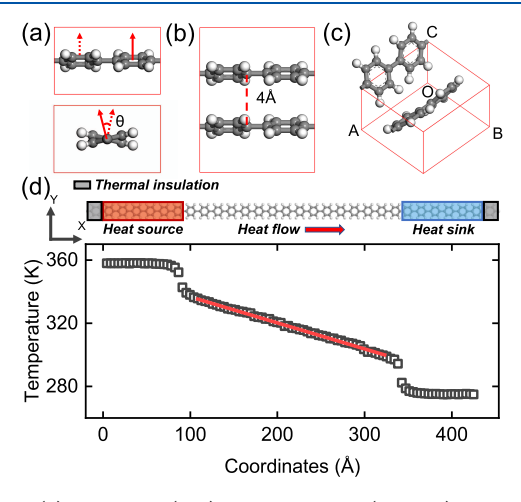


Figure 1. (a) Side view (top) and front view (bottom) of the single-chain PPP unit cell and the dihedral angle θ between two phenyl rings. (b) Unit cell of the double-chain PPP. (c) Unit cell and lattice vectors of the crystal PPP. (d) Top: NEMD simulation setup for the axial thermal conductivity of the single-chain PPP. Bottom: A typical simulated temperature profile of the single-chain PPP. The red solid line is the linear fitting of the temperature profile.

chain (referred to as "single chain" in this work). PPP is a conjugated polymer with an aromatic backbone where paraphenyl groups are connected in a head-to-tail configuration. Since the carbon atoms forming bonds between the phenyl groups have sp³ hybrid orbitals, the phenyl groups can rotate freely around the carbon—carbon bonds. The random rotation of the phenyl rings creates disorder in the single chain.

We used the dihedral angle θ between the phenyl rings to describe the relative positions of the rings. Figure 1b shows the atomic model of the double-chain configuration. The initial spacing between the two chains is set to be 4 Å because the distance between chains is 4.06 Å in the crystal cell along the OB axis (see Figure 1c). Figure 1c shows the unit cell of the PPP crystal. The lattice constants of PPP crystal are a=9.470 Å, b=8.120 Å, c=5.460 Å, $\alpha=90^\circ$, $\beta=90^\circ$, $\gamma=90^\circ$. The angle φ between the phenyl ring plane and the AC plane is 44.8° . In the unit cell, there are two PPP chains with two phenyl rings each.

To compute the thermal conductivity, we repeated the unit cell shown in Figure 1a–c in the axial direction (along the chain direction). For all configurations, we investigated five different lengths from 50 to 1000 segments, which correspond to from 21.7 to 434 nm. Here a segment is defined as a single phenyl ring. We did not repeat the cell in the radial direction (perpendicular to the chain direction) in the single-chain and double-chain configurations; we build a 2×2 supercell in the radial direction for the crystalline unit cell to ensure sufficient interchain interactions.⁵³

II.II. Molecular Dynamics (MD) Simulation for Thermal Conductivity. MD simulations can effectively capture the dynamic rotation of phenyl rings in PPP and have been employed in many previous investigations for understanding the thermal transport in polymer chains. We have used the same method as in our previous work, the nonequilibrium molecular dynamics (NEMD) simulations to calculate thermal conductivity, using the open-source LAMMPS package. 8,24,54,55 The interatomic potential (i.e., force field) is chosen as the Polymer Consistent Force Field (PCFF),56 which is one of the class II force fields for general all-atom descriptions of polymers and has been proved to be effective. Both the Lennard-Jones and Coulombic interactions have been considered to model the interchain interactions, including the $\pi - \pi$ interactions. All simulations used 0.25 fs as the time step, to capture the fast vibrations of carbon-hydrogen bonds. The force cutoff distance was set at 10 Å. For boundary conditions, a nonperiodic shrink-wrapping boundary style was used in the X direction (i.e., axial, along the chain direction) and periodic boundaries were used in the Y and Z directions. In single- and double-chain PPPs, the side length of the simulation box in both the Y and Z directions was set to 25 Å, to ensure the distance between the chains and their periodic images is much greater than the force cutoff distance.

Figure 1d (top) shows the schematic of the NEMD simulation setup. Details of applying this method on polymer systems can be found in our previous publications. 8,24,54,60 Briefly, the first phenyl ring at both ends of the chain was fixed at zero velocity to act as a thermal insulating wall (thermal insulation). The initial molecular configuration imported into LAMMPS has internal thermal stresses when heated, which can affect the simulation results. To relax the structure, the MD temperature of the whole molecular structure is maintained at 1 K for 50 ps to release the internal thermal stresses by employing an NVT (constant number of particles, volume, and temperature) ensemble. Then, the molecules are heated to the target MD simulation temperature, T, gradually by several NVT ensembles. Two Langevin thermostats are added to the heat sink and source regions (20 phenyl rings long) adjacent to the fixed rings at both ends to apply a thermal perturbation to the simulation domain. The temperatures of Langevin thermostats are set to (T + 15) and (T - 15) K to build the temperature gradient and generate heat flow along the molecules. A velocity-Verlet integration scheme corresponding to the "fix NVE" command in LAMMPS with a sufficiently long simulation time is performed to make the system reach the thermal steady state. After the system reaches the thermal steady state, another velocity-Verlet integration scheme with a 1 ns duration time is performed to collect the final simulation data. The average temperature and position of every atom and total energy injected into and removed out of the thermostats within the velocity-Verlet integration scheme are recorded during the run. The heat flux in the molecular chains is calculated as below

$$q = \frac{(E_{\text{hot}} + E_{\text{cold}})}{2 \times t \times A} \tag{1}$$

where $E_{\rm hot}$ is the energy injected to the heat source, $E_{\rm cold}$ is the energy removed out of the heat sink, t is the duration time in the last velocity-Verlet integration scheme, and A is the cross-sectional area. We set the cross-sectional area in the thermal conductivity calculation for a fair comparison among different dimensions, regardless of the real cross-sectional area in the MD simulation domain, which is intentionally enlarged to ensure the correct interchain coupling. The cross-sectional area of the single-chain PPP is set as $A_0 = 22.1676$ Å 2 (half of the cross-sectional area along the axial direction in the PPP crystal cell). For the double-chain and bulk-crystal PPP, the cross-sectional area is set as NA_0 , where N is the number of chains in the simulation domain.

Figure 1d (bottom) shows a typical temperature profile of the NEMD simulation, where a linear fit was used to calculate the temperature gradient in the linear region. The axial thermal conductivity of the PPP chain can be calculated by Fourier's law. Each reported thermal conductivity data point was averaged from the results of 10–20 MD simulations, where the uncertainties of the simulations were calculated.

We note here that we set the MD simulation temperature at *T*, which corresponds to a quantum-corrected temperature of 300 K. MD simulation uses the classical statistical description of heat capacity and kinetic energy

$$KE = \frac{\dim}{2} Nk_{\rm B}T \tag{2}$$

where KE is the total kinetic energy of the group of atoms, dim is the dimensionality of the simulation, N is the number of the group of atoms, $k_{\rm B}$ is the Boltzmann constant, and T is the temperature in the MD simulation. A quantum correction⁶¹ considers the temperature-dependent heat capacity using the Debye approximation. We solved the phonon density of states using the single-, double-chain, and crystal PPP structures and calculated the specific heat capacity and total kinetic energy as functions of temperature. By equating this quantum-corrected kinetic energy to the classic kinetic energy in eq 1, we can find the quantum-corrected temperature. Figure 2 shows the quantum-corrected temperature as a function of the MD simulation temperature. The temperature used in the MD simulations corresponds to a quantum-corrected temperature of ≈300 K and is slightly different among single-chain (53.7 K), double-chain (52.2 K), and crystal PPP (50.4 K).

III. RESULTS AND DISCUSSION

III.I. Anomalous Dependence of Thermal Conductivity on Dimensionality. Figure 3 shows the thermal

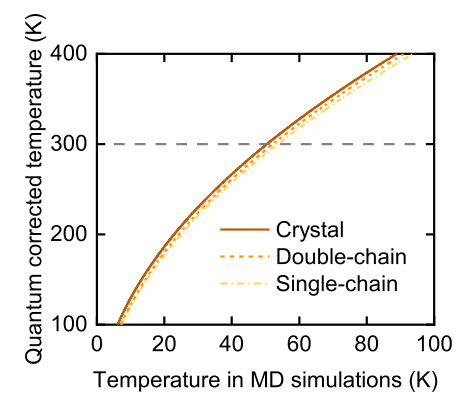


Figure 2. Quantum-corrected temperature as a function of the MD simulation temperature of single-chain (short dashed-dotted line), double-chain (short dashed line), and crystal (solid line) PPPs.

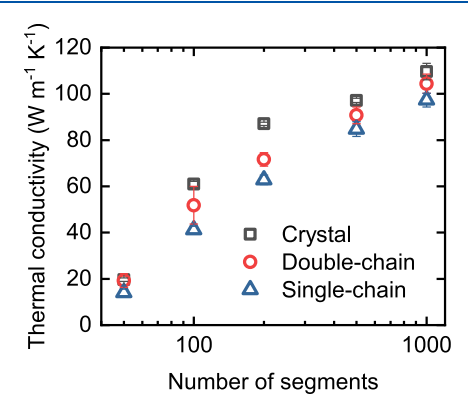


Figure 3. Axial thermal conductivity as a function of the number of segments in single-chain (triangle), double-chain (circle), and crystal (square) PPPs. The colored band represents the uncertainty of the simulation results.

conductivities of single-chain, double-chain, and crystal PPPs as a function of the number of segments (equivalent to the chain length). With increasing chain length, the thermal conductivity of these polymer chains shows a typical increasing trend, as shown in our previous work for other types of polymer chains.^{39,54} We note that when the number of segments reaches 1000 in crystal PPP, thermal conductivity seems to diverge with the chain length. This divergence trend may originate from the existence of long-wavelength phonons in low-dimensional systems or insufficient phonon scattering due to the small number of molecular chains for interchain anharmonic phonon scatterings. Nevertheless, in all lengths, the single-chain PPP possesses a significantly lower thermal conductivity compared to the double-chain and crystal PPP. Specifically, at the length of 100 segments, the single- and double-chain PPP have the thermal conductivity \approx 41.2 W m⁻¹ K^{-1} and ≈ 51.8 W m⁻¹ K⁻¹, respectively. The thermal conductivity of crystal PPP at the same length is ≈60.9 W m-1 K-1. This dimensionality dependence is in contrast with that in polymers with aliphatic backbone, such as PE⁴² and poly(dimethylsiloxane), 43 whose single-chain has a higher thermal conductivity than its double-chain and crystal counterparts.

In general, there are two possible effects of interchain interactions that cause the dimensionality dependence of thermal transport in polymer chains: (1) First, with the transition from one-dimensional (1D) to two-dimensional/

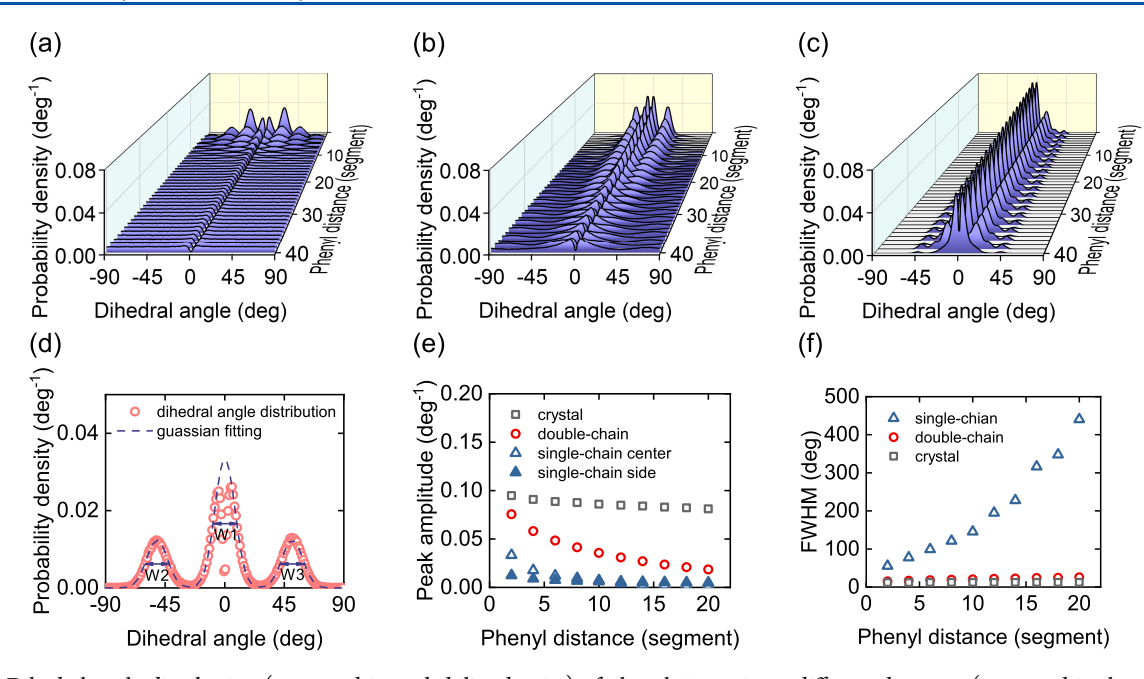


Figure 4. Dihedral angle distribution (expressed in probability density) of phenyl ring pairs at different distances (expressed in the unit of chain segments) in (a) single-chain, (b) double-chain, and (c) crystal PPP. (d) Gaussian distribution fitting on the dihedral angle distribution. (e) Amplitude of the dihedral angle distribution peak of the single-chain PPP at the center (hollow triangle) and side (solid triangle), double-chain PPP (hollow circle), and crystal PPP (hollow square). (f) Sum of full width at half-maximum (FWHM) of the single-chain (triangle), double-chain (circle), and crystal PPP (hollow square).

three-dimensional (2D/3D), the interchain interactions will induce strong anharmonic phonon scatterings between chains. Some of the phonon modes in the radial direction may directly scatter with the phonon modes in the axial direction, which will impede the heat transfer in the axial direction. (2) Second, the interchain interactions generate a confinement or steric effect so that the structure is more stable for thermal transport along the chains. The steric effect is generated from the nonbonded forces from all of the neighbor atoms and the balance of all forces. We believe that these two effects compete, generating different dimensionality dependences on thermal conductivity in polymer chains. In polymers with aliphatic backbones, such as PE and poly(dimethylsiloxane), the first effect likely dominates. We hypothesize that the second effect dominates in PPP so that an anomalous dimensionality dependence was observed.

III.II. Suppression of Free Rotation of Phenyl Rings with Interchain Interactions. Previous studies have revealed that in single extended chains, the random and free rotation of phenyl rings will disrupt the crystal periodicity of the molecular structure, which could affect both the phonon group velocity and mean free path. 54,62 To visualize and quantify the inhibition of free rotation of phenyl rings by interchain interactions, we analyzed the dihedral angle distribution of phenyl rings during the MD simulation. The dihedral angle is a geometric parameter used to describe the angle between two planes. In the PPP molecule, six carbon atoms in the same phenyl ring are in the same plane because of the π bond. By choosing three carbon atoms in one phenyl ring, we calculated the normal vector of the phenyl ring plane and the dihedral angle θ between two rings (shown in Figure 1a). The dihedral angle distribution describes the probability density as a function of the dihedral angle, which is statistically analyzed for dihedral angles between all of the phenyl ring pairs within the same polymer chain at each time step.

Figure 4 shows the dihedral angle distribution of phenyl rings of single-chain, double-chain, and crystal PPP at different distances between phenyl ring pairs. In the single-chain PPP shown in Figure 4a, only when the phenyl ring pair distance is less than 5 Å are significant peaks shown in the dihedral angle distribution. In other words, there is only a short-range order in the single-chain PPP when all of the phenyl rings can freely vibrate and rotate. As the nonbonded force decays rapidly with increasing distance between phenyl rings along the chain direction, the dihedral angle distribution becomes flat and broad due to the accumulation of random rotations over long distances. In double-chain PPP shown in Figure 4b, peaks occur in the dihedral angle distribution at the long-distance region and become sharper than those in the single-chain PPP, which indicates that the local random rotations have been suppressed by the interaction between PPP chains and the long-range order begins to form in the PPP chain. Figure 4c shows that almost all dihedral angles fall into the range within ±30° in crystal PPP and that the peaks extend to the longer phenyl ring distance range. The dihedral angle distribution peaks exhibit a higher amplitude and a lower width at the entire phenyl ring distance range in crystal PPP due to more pair interactions from all directions.

We note that all of the dihedral angle distribution curves have a deep valley at $\theta\approx 0^\circ$. The absence of the distribution of $\theta\approx 0^\circ$ is due to the repulsion of hydrogen atoms on phenyl rings and the random bending of the molecular chain. To quantify the backbone bending in the dynamic MD simulation, the orientational order parameter P2 of the 100-segments-long PPP chain is calculated to be 0.9955 (single-chain), 0.9960 (double-chain), and 0.9934 (crystal), using the method as in our previous publication, which indicates the average bending angle between the axial vectors is $\approx 3.5^\circ$.

To quantitatively compare the degree of long-range order of the PPP chain structure, we fit the dihedral angle distribution

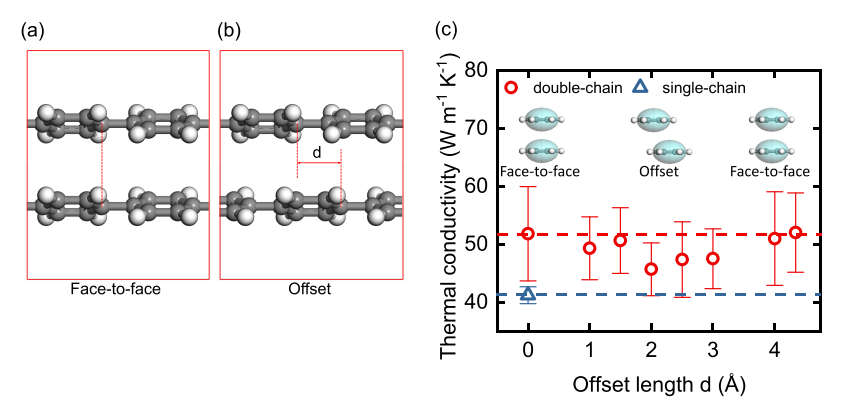


Figure 5. (a) Face-to-face double-chain PPP. (b) Offset double-chain PPP. (c) Axial thermal conductivity of the double-chain PPP model as a function of the offset length along the chain direction between a phenyl ring pair. The single-chain thermal conductivity is also presented as a dashed line for reference.

with a Gaussian distribution (shown in the Figure 4d) to measure the peak and the full width at half-maximum (FWHM) of the dihedral angle distribution. 64,65 With respect to any chosen phenyl ring of the PPP molecule in the crystal cell, the dihedral angles of the adjacent rings alternate between $\approx \pm 30$ and 0° . For example, the dihedral angle between the first and the second phenyl rings is $\approx \pm 30^{\circ}$, and the dihedral angle between the first and the third phenyl rings is $\approx 0^{\circ}$. When the dihedral angle is $\approx \pm 30^{\circ}$, The shape of the peaks is not symmetrical, so it is not easy to fit with a Gaussian distribution. For the sake of comparison, we treated the dihedral angle distribution curve as it has only one peak at $\approx 0^{\circ}$ (ignoring the small deep valley caused by the bending of the backbone) to fit the peak amplitude and the FWHM with the Gaussian distribution function as an example to quantitatively describe the arrangement of phenyl rings around the equilibrium position. In Figure 4f, we sum the FWHM's of all significant Gaussian distribution peaks as shown in Figure 4d. Figure 4e,f shows that the peak amplitude and the FWHM of the dihedral angle distribution have the highest and the lowest values at the shortest distance, respectively, which indicates that the order by counting only the phenyl rings at the nearest neighbor (i.e., short-range order) is more pronounced. In contrast, the longrange order is defined as the phenyl rings demonstrating a similar spatial arrangement periodically after a long-enough distance in the PPP chain. With an increasing distance, the peak decreases and the FWHM increases in all three models. Note that the peak amplitude of the dihedral angle probability in the single-chain PPP reaches down to the uniform distribution magnitude (0.0056 deg⁻¹) as the distance gradually increases. This fact implies that only short-range order exists in the single-chain PPP when the number of chain segments is more than 10. In the double-chain and bulk PPP, the peak amplitude maintains levels above 0.02 and 0.08 deg⁻¹, respectively, for the phenyl ring distance within 20 segments. The FWHM also converges over long distances in the doublechain and bulk PPP. These comparison results indicate that the interaction from other neighboring chains restricts the rotation of phenyl rings and provides the double-chain and bulk PPP with the long-range order. Even at the nearest distance, the interaction from other chains also increases the dihedral angle probability and improves the short-range order.

The analysis in Figure 4 confirms the strong correlation between the spatial order of the phenyl rings in the molecular chain and the axial thermal conductivity. When phenyl rings are orderly arranged in molecules, the axial thermal conductivity can be effectively improved compared to that of a molecule with only a short-range order. Even with sufficient short- and long-range ordering, further enhancing the molecular interchain constraints to improve the ordering within their respective spatial ranges can still lead to a continued improvement in the axial thermal transport efficiency of the molecular chains. As shown in Figure 3, crystal PPPs have a higher thermal conductivity compared with double-chain PPPs with a length from 100 to 1000 segments while crystal PPP has a dihedral angle distribution with a higher amplitude and a lower FWHM indicating a more ordered structure (shown in Figure 4).

III.III. Role of $\pi-\pi$ Stacking. All of the results and analysis in Sections III.I and III.II confirm that the role of the interchain interactions on the thermal transport in PPP systems is dominantly by suppressing the free rotation of phenyl rings and promoting the long-range order. The interchain interactions do not seem to facilitate strong phonon scatterings among modes in the chain axial and radial directions. This conclusion seems counterintuitive. Intuitively, a stacking structure due to the orbital overlap should enhance thermal transport between the aromatic rings due to the stronger bonding strength and even affect the thermal transport along the aromatic chains. Yet, our results indicate the opposite.

In this section, we investigated the role of $\pi - \pi$ stacking in thermal transport. In chemical structures with aromatic rings, three types of $\pi - \pi$ stacking are commonly observed: (1) face-to-face (also called sandwich), (2) offset (also called parallel-displaced or staggered), and (3) T-shaped (also called edge-to-face). In this work, we study the effect of the first two types of π - π stacking on the thermal transport in PPP chains, which is relevant in the study of dimensionality dependence. As shown in the inset of Figure 5, the face-to-face type represents a direct stacking of the two phenyl rings with a sandwich-style overlap. In this type, the carbon atoms with partial negative charges from one ring are on top of other partial negatively charged carbon atoms from the second ring; the hydrogen atoms with partial positive charges are on top of other hydrogen atoms that likewise carry partial positive charges. The forces between the rings therefore are dominated by strong repulsive forces. The offset type represents a paralleldisplaced arrangement of phenyl rings, and the overlapping area is not equal to the total phenyl ring area. The carbon

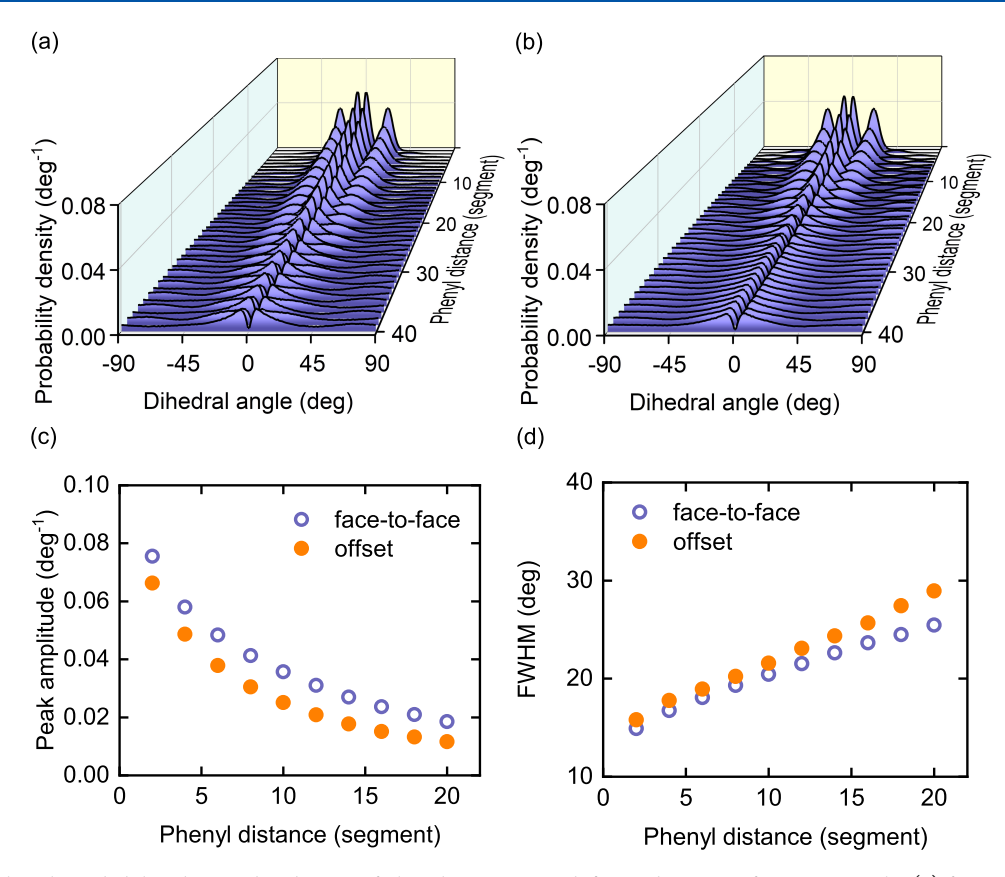


Figure 6. Dihedral angle probability density distribution of phenyl ring pairs at different distances of segments in the (a) face-to-face and (b) offset double-chain PPPs. (c) Peak amplitude and (d) FWHM of the face-to-face (hollow circle) and offset (solid circle) double-chain PPPs.

atoms with a partial negative charge in the first ring are placed above hydrogen atoms with a partial positive charge in the second ring so that the forces between the rings become attractive. The offset stacking, with a weaker interaction strength, is more energetically favorable than face-to-face stacking. Presumably, if the effect of interchain interactions is dominated by the structural short-range and long-range order enforced by the interactions, the thermal conductivity will decrease from the face-to-face stacking to offset stacking; if the effect of interchain interactions is dominated by the interchain phonon scattering, the thermal conductivity will increase from the face-to-face stacking to offset stacking because of a weaker interaction strength and less coupling in the offset stacking.

To investigate the effect of $\pi - \pi$ stacking type on the axial thermal conductivity of double-chain PPP, we performed a series of NEMD simulations of double-chain PPPs by systematically offsetting one chain in the sideways direction from 0 to 4.34 Å (i.e., one segment length). The type of $\pi - \pi$ stacking will gradually change from face-to-face to offset and then to face-to-face again from the originally paired ring to the next ring as a function of the offset length. Figure 6 shows that the axial thermal conductivity of the double-chain PPP decreases first when the offset length varies from 0 to 2 Å and then increases again to the original value when the offset length continues to increase from 2 to 4.34 Å. The reduction of thermal conductivity is maximized at an offset length 2 Å, which is only $\approx 15\%$. Note that the reduction of thermal conductivity from the double-chain to single-chain configuration is $\approx 27\%$.

To elucidate whether the reduction of the axial thermal conductivity is due to increased chain disorder, we analyzed the dihedral angle distribution of the face-to-face and offset types of double-chain PPPs. Figure 6 shows that the peak of the dihedral angle distribution of the offset double-chain PPP is lower than that of the face-to-face one, and its FWHM is larger than that of the face-to-face one, which indicates the local disorder is slightly stronger in the offset case. Therefore, the phonon scattering along the chain direction should be stronger due to the rotational disorder and causes a slight decrease of thermal conductivity in the offset double-chain PPP. This result again supports that the enhancement (suppression) of thermal conductivity can be correlated with the π - π stacking-induced relative structural order (disorder) along the chain direction.

To understand the thermal transport across phenyl rings, we followed the same method as in our previous work to calculate the thermal conductance between PPP and PE double-chains (shown in Figure 7). In this simulation, two polymer chains with a spacing distance of 4 Å are fixed at both ends; the inner ends of the two polymer chains are overlapped with a certain length L. Thermal reservoirs are applied on the nonoverlapping regions to impose a temperature difference and create the heat flow across the molecules interface. The thermal conductance (G) between the PPP (or PE) chains is defined as follows:

$$G = \frac{Q}{wL\Delta T} \tag{3}$$

where Q is the heat flow across the interface, w is the width of the PPP (or PE) molecules, L is the length of the overlapping region, and ΔT is the average temperature along the overlapping region. The width of the PPP molecules is set to

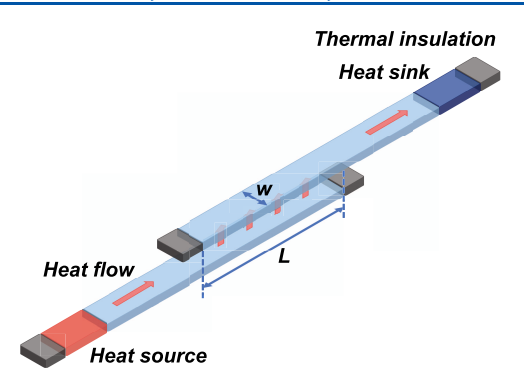


Figure 7. Schematic diagram of the setup for calculating the thermal conductance across overlapping polymer chains equipped with two thermal insulating ends.

be the same as the lattice constant c of the crystal PPP (5.460 Å). The width of the PE molecules is set to be the square root of the cross-sectional area for the single chain (4.267 Å). The overlapping length of the face-to-face type is equal to the integer multiple of the unit cell length (4.340 Å for PPP and 2.507 Å for PE). Based on the face-to-face type overlapped PPP, we move one of the two chains half of the unit cell length further to switch the $\pi-\pi$ stacking to the offset type.

Figure 8a shows the interchain thermal conductance as a function of the overlapping length in two types of $\pi-\pi$ stacking. The interchain thermal conductance in PPP of both types is about three times smaller than that in PE. As the

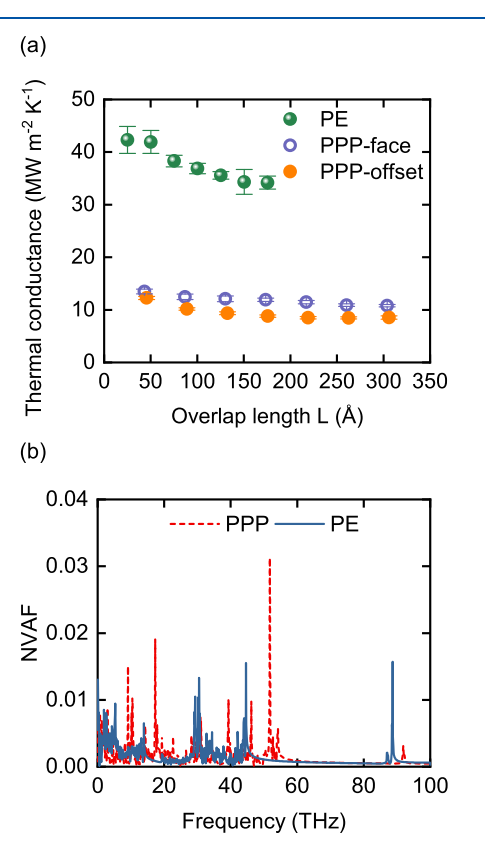


Figure 8. (a) Thermal conductance across two polymer chains as a function of the overlapping length in PE (green ball), face-to-face type PPP (purple hollow circle), and offset type PPP (orange solid circle). (b) Densities of vibrational normal modes of double-chain PE (solid line) and PPP (short dash).

overlapping length increases, the thermal conductance difference between the face-to-face and offset types increases from ≈ 10 to $\approx 35\%$. In general, the interchain thermal conductance of the offset type is lower than that of the face-to-face type, which will lead to a further reduction in the degree of already-weak thermal coupling between phonons traveling along the axial and radial directions. In conclusion, the decrease in the axial thermal conductivity of the PPP double-chain caused by the shift from the face-to-face type to the offset type of $\pi-\pi$ stacking is mainly dominated by the chain disorder, while the weakening of interchain phonon coupling is not strong enough to counteract the effect of chain disorder.

Last, we examine the seemingly counterintuitive result that the interchain thermal conductance is more than three times lower across PPP chains than in the PE chains, considering their stronger interchain bonding strength due to $\pi - \pi$ stacking. To understand such a significant thermal conductance difference, we calculated the density of vibrational normal modes by performing a fast Fourier transform on the normalized velocity autocorrelation functions (NVAFs) from atoms at the overlapped region, as in our previous publication. The NVAF was calculated as below

$$NVAF = \frac{\langle \nu(t) \cdot \nu(0) \rangle}{\langle \nu(0) \cdot \nu(0) \rangle}$$
(4)

where v(t) is the velocity vector of atom at time t, $\langle \ \rangle$ denotes the ensemble average, and the numerator term is expressed as below

$$\langle \mathbf{v}(t) \cdot \mathbf{v}(0) \rangle = \frac{1}{M} \sum_{j=1}^{M} \frac{1}{N} \sum_{i=1}^{N} \mathbf{v}_{j,i} \cdot \mathbf{v}_{j,i+t/\Delta t}$$
(5)

where $v_{j,i}$ represents the velocity vector of atom j at time step i. The region where we chose for the NVAF's calculation is in the region of two parallel and overlapped polymer fragments, which contain 36 carbon atoms in the double-chain PE and 48 carbon atoms in the double-chain PPP, respectively. We consider only the contribution from the vibrational modes of carbon atoms in the NVAFs. While the time step between adjacent atom velocity vectors is set as 5 fs and the total sampling time is set as 10 ps, the resolution of the output spectrum is 0.1 THz, and the maximum frequency is 100 THz.

Figure 8b shows that the normal modes of double-chain PPP are highly concentrated on selected frequencies and relatively absent between these major frequencies. The relatively sharp peaks merge from a background of zero density (even at low frequencies) as if the normal modes have been "filtered". On the contrary, normal modes of the double-chain PE show a continuous spectrum that covers almost all frequencies below 60 THz and barely has normal modes with zero density. The availability of many vibrational modes that can participate in the mode coupling in the PE double-chain will significantly enhance the interchain thermal conductance, but at the same time, possibly also enable the "crosstalk" between the modes along the chains and across the chains. The lack of sufficient modes with diverse vibrational frequencies in the PPP doublechain qualitatively explains the much lower interchain thermal conductance and a weaker coupling between the modes along the chains and across the chains.

IV. CONCLUSIONS

A series of MD simulations were performed to study the axial thermal conductivity of PPP in different dimensions. The result shows that the double-chain and crystal PPP have higher axial thermal conductivities than the single-chain PPP, which is in direct contrast with aliphatic backbone polymer chains, such as PE. The planar and rigid rings in the aromatic backbone and their rotational freedom contribute to this anomalous dimensionality dependence of thermal conductivity in PPP. From the single-chain to double-chain or crystal PPP, suppression of random rotation of rings by $\pi-\pi$ stacking improves both short-range and long-range structural orders. Meanwhile, the axial thermal conductivity is also related to the π - π stacking type. We also found that stronger π - π stacking does not necessarily lead to a higher intermolecular thermal conductance. This work reports a different dimensional dependence from the current literature on molecular chains and clarifies that this anomalous dimensional dependence is attributed to the unique intermolecular interactions between phenyl rings. Moreover, this work can inspire future work on molecular engineering of thermal conductivity in polymers by utilizing $\pi - \pi$ stacking in the conjugated polymers.

AUTHOR INFORMATION

Corresponding Authors

Xiaobo Li — School of Energy and Power Engineering, Huazhong University of Science and Technology, Wuhan 430074, China; Email: xbli35@hust.edu.cn

Jun Liu — Department of Mechanical and Aerospace Engineering, North Carolina State University, Raleigh, North Carolina 27695, United States; Email: jliu38@ncsu.edu

Authors

Cong Yang – Department of Mechanical and Aerospace Engineering, North Carolina State University, Raleigh, North Carolina 27695, United States

Saqlain Raza – Department of Mechanical and Aerospace Engineering, North Carolina State University, Raleigh, North Carolina 27695, United States

Complete contact information is available at: https://pubs.acs.org/10.1021/acs.jpcb.3c02947

Notes

The authors declare no competing financial interest.

■ ACKNOWLEDGMENTS

Computational resources were provided by the High-Performance Computing Center at North Carolina State University and the Advanced Cyberinfrastructure Coordination Ecosystem: Service & Support (ACCESS) program, which is supported by NSF grants 2138259, 2138286, 2138307, 2137603, and 2138296. C.Y., S.R., and J.L. acknowledge the financial support from the National Science Foundation under the award number CBET 1943813.

REFERENCES

- (1) Tomko, J. A.; Pena-Francesch, A.; Jung, H.; Tyagi, M.; Allen, B. D.; Demirel, M. C.; Hopkins, P. E. Tunable Thermal Transport and Reversible Thermal Conductivity Switching in Topologically Networked Bio-Inspired Materials. *Nat. Nanotechnol.* **2018**, *13* (10), 959–964.
- (2) Shin, J.; Sung, J.; Kang, M.; Xie, X.; Lee, B.; Lee, K. M.; White, T. J.; Leal, C.; Sottos, N. R.; Braun, P. V.; Cahill, D. G. Light-

- Triggered Thermal Conductivity Switching in Azobenzene Polymers. *Proc. Natl. Acad. Sci. U.S.A.* **2019**, *116* (13), 5973–5978.
- (3) Li, C.; Ma, Y.; Tian, Z. Thermal Switching of Thermoresponsive Polymer Aqueous Solutions. ACS Macro Lett. 2018, 7 (1), 53–58.
- (4) Sun, B.; Huang, X. Seeking Advanced Thermal Management for Stretchable Electronics. *Npj Flex. Electron.* **2021**, *5* (1), No. 12.
- (5) Li, X.; Xie, W.; Sui, C.; Hsu, P.-C. Multispectral Thermal Management Designs for Net-Zero Energy Buildings. *ACS Mater. Lett.* **2020**, 2 (12), 1624–1643.
- (6) Wu, C.-W.; Ren, X.; Zhou, W.-X.; Xie, G.; Zhang, G. Thermal Stability and Thermal Conductivity of Solid Electrolytes. *APL Mater.* **2022**, *10* (4), No. 040902.
- (7) Henry, A. Thermal Transport in Polymers. *Annu. Rev. Heat Transfer* **2014**, 17, 485–520.
- (8) He, J.; Liu, J. Molecular Dynamics Simulation of Thermal Transport in Semicrystalline Polyethylene: Roles of Strain and the Crystalline-Amorphous Interphase Region. *J. Appl. Phys.* **2021**, *130* (22), No. 225101.
- (9) Wang, X.; Kaviany, M.; Huang, B. Phonon Coupling and Transport in Individual Polyethylene Chains: A Comparison Study with the Bulk Crystal. *Nanoscale* **2017**, 9 (45), 18022–18031.
- (10) Kim, T.; Drakopoulos, S. X.; Ronca, S.; Minnich, A. J. Origin of High Thermal Conductivity in Disentangled Ultra-High Molecular Weight Polyethylene Films: Ballistic Phonons within Enlarged Crystals. *Nat. Commun.* **2022**, *13* (1), No. 2452.
- (11) Xu, Y.; Kraemer, D.; Song, B.; Jiang, Z.; Zhou, J.; Loomis, J.; Wang, J.; Li, M.; Ghasemi, H.; Huang, X.; et al. Nanostructured Polymer Films with Metal-like Thermal Conductivity. *Nat. Commun.* **2019**, *10* (1), No. 1771.
- (12) Xu, Y.; Wang, X.; Zhou, J.; Song, B.; Jiang, Z.; Lee, E. M. Y.; Huberman, S.; Gleason, K. K.; Chen, G. Molecular Engineered Conjugated Polymer with High Thermal Conductivity. *Sci. Adv.* **2018**, 4 (3), No. eaar3031.
- (13) Peng, Z.; Ye, L.; Ade, H. Understanding, Quantifying, and Controlling the Molecular Ordering of Semiconducting Polymers: From Novices to Experts and Amorphous to Perfect Crystals. *Mater. Horiz.* **2022**, *9* (2), 577–606.
- (14) Zhu, M.-X.; Song, H.-G.; Yu, Q.-C.; Chen, J.-M.; Zhang, H.-Y. Machine-Learning-Driven Discovery of Polymers Molecular Structures with High Thermal Conductivity. *Int. J. Heat Mass Transfer* **2020**, *162*, No. 120381.
- (15) Zhou, T.; Wu, Z.; Chilukoti, H. K.; Müller-Plathe, F. Sequence-Engineering Polyethylene—Polypropylene Copolymers with High Thermal Conductivity Using a Molecular-Dynamics-Based Genetic Algorithm. *J. Chem. Theory Comput.* **2021**, *17* (6), 3772–3782.
- (16) Nagoya, A.; Kikkawa, N.; Ohba, N.; Baba, T.; Kajita, S.; Yanai, K.; Takeno, T. Autonomous Search for Polymers with High Thermal Conductivity Using a Rapid Green–Kubo Estimation. *Macromolecules* **2022**, *55* (9), 3384–3395.
- (17) Ma, R.; Zhang, H.; Xu, J.; Sun, L.; Hayashi, Y.; Yoshida, R.; Shiomi, J.; Wang, J.; Luo, T. Machine Learning-Assisted Exploration of Thermally Conductive Polymers Based on High-Throughput Molecular Dynamics Simulations. *Mater. Today Phys.* **2022**, *28*, No. 100850.
- (18) Choy, C. L.; Luk, W. H.; Chen, F. C. Thermal Conductivity of Highly Oriented Polyethylene. *Polymer* 1978, 19 (2), 155–162.
- (19) Choy, C. L.; Chen, F. C.; Luk, W. H. Thermal Conductivity of Oriented Crystalline Polymers. *J. Polym. Sci., Polym. Phys. Ed.* **1980**, *18* (6), 1187–1207.
- (20) Liu, J.; Yang, R. Tuning the Thermal Conductivity of Polymers with Mechanical Strains. *Phys. Rev. B* **2010**, *81* (17), No. 174122.
- (21) Lv, G.; Jensen, E.; Shan, N.; Evans, C. M.; Cahill, D. G. Effect of Aromatic/Aliphatic Structure and Cross-Linking Density on the Thermal Conductivity of Epoxy Resins. *ACS Appl. Polym. Mater.* **2021**, *3* (3), 1555–1562.
- (22) Ma, H.; Tian, Z. Effects of Polymer Topology and Morphology on Thermal Transport: A Molecular Dynamics Study of Bottlebrush Polymers. *Appl. Phys. Lett.* **2017**, *110* (9), No. 091903.

- (23) Tu, R.; Liao, Q.; Zeng, L.; Liu, Z.; Liu, W. Impact of Torsion and Stretching on the Thermal Conductivity of Polyethylene Strands. *Appl. Phys. Lett.* **2017**, *110* (10), No. 101905.
- (24) Duan, X.; Li, Z.; Liu, J.; Chen, G.; Li, X. Roles of Kink on the Thermal Transport in Single Polyethylene Chains. *J. Appl. Phys.* **2019**, 125 (16), No. 164303.
- (25) Zhang, T.; Luo, T. Role of Chain Morphology and Stiffness in Thermal Conductivity of Amorphous Polymers. *J. Phys. Chem. B* **2016**, *120* (4), 803–812.
- (26) Lu, T.; Kim, K.; Li, X.; Zhou, J.; Chen, G.; Liu, J. Thermal Transport in Semicrystalline Polyethylene by Molecular Dynamics Simulation. *J. Appl. Phys.* **2018**, *123* (1), No. 015107.
- (27) Zhang, T.; Luo, T. Morphology-Influenced Thermal Conductivity of Polyethylene Single Chains and Crystalline Fibers. *J. Appl. Phys.* **2012**, *112* (9), No. 094304.
- (28) Hu, J.; Liu, B.; Subramanyan, H.; Li, B.; Zhou, J.; Liu, J. Enhanced Thermoelectric Properties through Minority Carriers Blocking in Nanocomposites. *J. Appl. Phys.* **2019**, *126* (9), No. 095107.
- (29) Lv, G.; Li, X.; Jensen, E.; Soman, B.; Tsao, Y.-H.; Evans, C. M.; Cahill, D. G. Dynamic Covalent Bonds in Vitrimers Enable 1.0 W/(m K) Intrinsic Thermal Conductivity. *Macromolecules* **2023**, *56* (4), 1554–1561.
- (30) Lv, G.; Shen, C.; Shan, N.; Jensen, E.; Li, X.; Evans, C. M.; Cahill, D. G. Odd–Even Effect on the Thermal Conductivity of Liquid Crystalline Epoxy Resins. *Proc. Natl. Acad. Sci. U.S.A.* **2022**, 119 (46), No. e2211151119.
- (31) Lv, G.; Soman, B.; Shan, N.; Evans, C. M.; Cahill, D. G. Effect of Linker Length and Temperature on the Thermal Conductivity of Ethylene Dynamic Networks. *ACS Macro Lett.* **2021**, *10* (9), 1088–1093
- (32) Wei, X.; Zhang, T.; Luo, T. Chain Conformation-Dependent Thermal Conductivity of Amorphous Polymer Blends: The Impact of Inter- and Intra-Chain Interactions. *Phys. Chem. Chem. Phys.* **2016**, *18* (47), 32146–32154.
- (33) Kim, G.-H.; Lee, D.; Shanker, A.; Shao, L.; Kwon, M. S.; Gidley, D.; Kim, J.; Pipe, K. P. High Thermal Conductivity in Amorphous Polymer Blends by Engineered Interchain Interactions. *Nat. Mater.* **2015**, *14* (3), 295–300.
- (34) Wei, X.; Wang, Z.; Tian, Z.; Luo, T. Thermal Transport in Polymers: A Review. J. Heat Transfer 2021, 143 (7), No. 072101.
- (35) Guo, Y.; Zhou, Y.; Xu, Y. Engineering Polymers with Metal-like Thermal Conductivity—Present Status and Future Perspectives. *Polymer* **2021**, 233, No. 124168.
- (36) Huang, C.; Qian, X.; Yang, R. Thermal Conductivity of Polymers and Polymer Nanocomposites. *Mater. Sci. Eng., R* **2018**, *132*, 1–22.
- (37) Xu, Y.; Wang, X.; Hao, Q. A Mini Review on Thermally Conductive Polymers and Polymer-Based Composites. *Compos. Commun.* **2021**, 24, No. 100617.
- (38) Xu, X.; Chen, J.; Zhou, J.; Li, B. Thermal Conductivity of Polymers and Their Nanocomposites. *Adv. Mater.* **2018**, 30 (17), No. 1705544.
- (39) Henry, A.; Chen, G. High Thermal Conductivity of Single Polyethylene Chains Using Molecular Dynamics Simulations. *Phys. Rev. Lett.* **2008**, *101* (23), No. 235502.
- (40) Shen, S.; Henry, A.; Tong, J.; Zheng, R.; Chen, G. Polyethylene Nanofibres with Very High Thermal Conductivities. *Nat. Nanotechnol.* **2010**, *5* (4), 251–255.
- (41) Shrestha, R.; Li, P.; Chatterjee, B.; Zheng, T.; Wu, X.; Liu, Z.; Luo, T.; Choi, S.; Hippalgaonkar, K.; de Boer, M. P.; Shen, S. Crystalline Polymer Nanofibers with Ultra-High Strength and Thermal Conductivity. *Nat. Commun.* **2018**, *9* (1), No. 1664.
- (42) Henry, A.; Chen, G.; Plimpton, S. J.; Thompson, A. 1D-to-3D Transition of Phonon Heat Conduction in Polyethylene Using Molecular Dynamics Simulations. *Phys. Rev. B* **2010**, 82 (14), No. 144308.

- (43) Luo, T.; Esfarjani, K.; Shiomi, J.; Henry, A.; Chen, G. Molecular Dynamics Simulation of Thermal Energy Transport in Polydimethylsiloxane. *J. Appl. Phys.* **2011**, *109* (7), No. 074321.
- (44) Gu, X.; Wei, Y.; Yin, X.; Li, B.; Yang, R. Colloquium: Phononic Thermal Properties of Two-Dimensional Materials. *Rev. Mod. Phys.* **2018**, *90* (4), No. 041002.
- (45) Singh, D.; Murthy, J. Y.; Fisher, T. S. Mechanism of Thermal Conductivity Reduction in Few-Layer Graphene. *J. Appl. Phys.* **2011**, 110 (4), No. 044317.
- (46) Gu, X.; Li, B.; Yang, R. Layer Thickness-Dependent Phonon Properties and Thermal Conductivity of MoS2. *J. Appl. Phys.* **2016**, 119 (8), No. 085106.
- (47) Luo, Z.; Maassen, J.; Deng, Y.; Du, Y.; Garrelts, R. P.; Lundstrom, M. S.; Ye, P. D.; Xu, X. Anisotropic In-Plane Thermal Conductivity Observed in Few-Layer Black Phosphorus. *Nat. Commun.* **2015**, *6* (1), No. 8572.
- (48) Thakuria, R.; Nath, N. K.; Saha, B. K. The Nature and Applications of π – π Interactions: A Perspective. *Cryst. Growth Des.* **2019**, 19 (2), 523–528.
- (49) Chen, T.; Li, M.; Liu, J. $\pi-\pi$ Stacking Interaction: A Nondestructive and Facile Means in Material Engineering for Bioapplications. *Cryst. Growth Des.* **2018**, *18* (5), 2765–2783.
- (50) Cai, W.; Xu, D.; Qian, L.; Wei, J.; Xiao, C.; Qian, L.; Lu, Z.; Cui, S. Force-Induced Transition of $\pi-\pi$ Stacking in a Single Polystyrene Chain. *J. Am. Chem. Soc.* **2019**, *141* (24), 9500–9503.
- (51) Zhang, T.; Wu, X.; Luo, T. Polymer Nanofibers with Outstanding Thermal Conductivity and Thermal Stability: Fundamental Linkage between Molecular Characteristics and Macroscopic Thermal Properties. J. Phys. Chem. C 2014, 118 (36), 21148–21159.
- (52) Ambrosch-Draxl, C.; Majewski, J. A.; Vogl, P.; Leising, G. First-Principles Studies of the Structural and Optical Properties of Crystalline Poly (Para-Phenylene). *Phys. Rev. B* **1995**, *51* (15), 9668.
- (53) Hu, L.; Evans, W. J.; Keblinski, P. One-Dimensional Phonon Effects in Direct Molecular Dynamics Method for Thermal Conductivity Determination. *J. Appl. Phys.* **2011**, *110* (11), No. 113511.
- (54) Liu, J.; Yang, R. Length-Dependent Thermal Conductivity of Single Extended Polymer Chains. *Phys. Rev. B* **2012**, *86* (10), No. 104307.
- (55) Subramanyan, H.; Zhang, W.; He, J.; Kim, K.; Li, X.; Liu, J. Role of Angular Bending Freedom in Regulating Thermal Transport in Polymers. *J. Appl. Phys.* **2019**, *125* (9), No. 095104.
- (56) Sun, H.; Mumby, S. J.; Maple, J. R.; Hagler, A. T. An Ab Initio CFF93 All-Atom Force Field for Polycarbonates. *J. Am. Chem. Soc.* **1994**, *116* (7), 2978–2987.
- (57) Sun, H. Force Field for Computation of Conformational Energies, Structures, and Vibrational Frequencies of Aromatic Polyesters. *J. Comput. Chem.* **1994**, *15* (7), 752–768.
- (58) Hill, J. R.; Sauer, J. Molecular Mechanics Potential for Silica and Zeolite Catalysts Based on Ab Initio Calculations. 1. Dense and Microporous Silica. *J. Phys. Chem. A* **1994**, *98* (4), 1238–1244.
- (59) Sun, H. Ab Initio Calculations and Force Field Development for Computer Simulation of Polysilanes. *Macromolecules* **1995**, 28 (3), 701–712.
- (60) Yang, C.; Duan, X.; Zhou, J.; Liu, J.; Li, X. Thermal Transport across Polyethylene Chains. J. Therm. Sci. 2022, 31 (4), 1061–1067.
- (61) Cahill, D. G.; Ford, W. K.; Goodson, K. E.; Mahan, G. D.; Majumdar, A.; Maris, H. J.; Merlin, R.; Phillpot, S. R. Nanoscale Thermal Transport. *J. Appl. Phys.* **2003**, *93* (2), 793–818.
- (62) Ma, H.; Tian, Z. Chain Rotation Significantly Reduces Thermal Conductivity of Single-Chain Polymers. *J. Mater. Res.* **2019**, 34 (1), 126–133.
- (63) Lafrance, C.-P.; Nabet, A.; Prud'homme, R. E.; Pézolet, M. On the Relationship between the Order Parameter and the Shape of Orientation Distributions. *Can. J. Chem.* **1995**, 73 (9), 1497–1505.
- (64) He, J.; Liu, J. Evaluating the Roles of Temperature-Dependent Eigenvectors in Predicting Phonon Transport Properties of Anharmonic Crystals Using Normal Mode Analysis Methods. *J. Appl. Phys.* **2021**, 129 (21), No. 215102.

- (65) He, J.; Kim, K.; Wang, Y.; Liu, J. Strain Effects on the Anisotropic Thermal Transport in Crystalline Polyethylene. *Appl. Phys. Lett.* **2018**, *112* (5), No. 051907.
- (66) Liu, J.; Alhashme, M.; Yang, R. Thermal Transport across Carbon Nanotubes Connected by Molecular Linkers. *Carbon* **2012**, 50 (3), 1063–1070.